


Coronavirus pleomorphism


Cite as: Phys. Fluids **34**, 063101 (2022); <https://doi.org/10.1063/5.0094771>

Submitted: 06 April 2022 • Accepted: 15 April 2022 • Accepted Manuscript Online: 10 May 2022 •
Published Online: 02 June 2022

 M. A. Kanso, M. Naime, V. Chaurasia, et al.

COLLECTIONS

 This paper was selected as Featured

 This paper was selected as Scilight



View Online



Export Citation



CrossMark

ARTICLES YOU MAY BE INTERESTED IN

[Assessing effectiveness and comfortability of a two-layer cloth mask with a high-efficiency particulate air \(HEPA\) insert to mitigate COVID-19 transmission](#)

Phys. Fluids **34**, 061703 (2022); <https://doi.org/10.1063/5.0094116>

[Coronavirus shape alters infection ability](#)

Scilight **2022**, 221109 (2022); <https://doi.org/10.1063/10.0011625>

[Oscillatory behavior with fiber orientation in the flow-vorticity plane for fiber suspension under large amplitude oscillatory shear flow](#)

Phys. Fluids **34**, 063102 (2022); <https://doi.org/10.1063/5.0092088>

APL Machine Learning

Open, quality research for the networking communities

MEET OUR NEW EDITOR-IN-CHIEF

LEARN MORE



Coronavirus pleomorphism

Cite as: Phys. Fluids **34**, 063101 (2022); doi: 10.1063/5.0094771

Submitted: 6 April 2022 · Accepted: 15 April 2022 ·

Published Online: 2 June 2022



View Online



Export Citation



CrossMark

M. A. Kanso,¹  M. Naime,² V. Chaurasia,³ K. Tontiwattanakul,⁴  E. Fried,³  and A. J. Giacomin^{1,5,6,a)} 

AFFILIATIONS

¹Chemical Engineering Department, Polymers Research Group, Queen's University, Kingston, Ontario K7L 3N6, Canada

²Chemical Engineering Department, American University of Beirut, Lebanon

³Okinawa Institute of Science and Technology, Tancha, Onna, Kunigami District, Okinawa 904-0495, Japan

⁴Department of Mechanical and Aerospace Engineering, King Mongkut's University of Technology North Bangkok, Thailand

⁵Mechanical and Materials Engineering Department, Queen's University, Kingston, Ontario K7L 3N6, Canada

⁶Physics, Engineering Physics and Astronomy Department, Queen's University, Kingston, Ontario K7L 3N6, Canada

^{a)}Author to whom correspondence should be addressed: giacomin@queensu.ca

ABSTRACT

The coronavirus is always idealized as a spherical capsid with radially protruding spikes. However, histologically, in the tissues of infected patients, capsids in cross section are elliptical, and only sometimes spherical [Neuman *et al.*, "Supramolecular architecture of severe acute respiratory syndrome coronavirus revealed by electron cryomicroscopy," *J Virol*, **80**, 7918 (2006)]. This capsid ellipticity implies that coronaviruses are oblate or prolate or both. We call this diversity of shapes, pleomorphism. Recently, the rotational diffusivity of the spherical coronavirus in suspension was calculated, from first principles, using general rigid bead-rod theory [Kanso *et al.*, "Coronavirus rotational diffusivity," *Phys Fluids* **32**, 113101 (2020)]. We did so by beading the spherical capsid and then also by replacing each of its bulbous spikes with a single bead. In this paper, we use energy minimization for the spreading of the spikes, charged identically, over the oblate or prolate capsids. We use general rigid bead-rod theory to explore the role of such coronavirus cross-sectional ellipticity on its rotational diffusivity, the transport property around which its cell attachment revolves. We learn that coronavirus ellipticity drastically decreases its rotational diffusivity, be it oblate or prolate.

Published under an exclusive license by AIP Publishing. <https://doi.org/10.1063/5.0094771>

I. INTRODUCTION

The coronavirus is thought of as a spherical capsid with radially protruding spikes. However, histologically, in the tissues of infected patients, capsids in cross section are aspherical, roughly elliptical, and only sometimes spherical. For instance, its capsid may be elliptical when microtomed in preparation for microscopy (see all 35 panels of Fig. 2 of Ref. 1, which we reproduce here in Fig. 1). This capsid ellipticity implies that coronaviruses are oblate or prolate or both. We call this diversity of shapes, pleomorphism. We know of no live microscopy of the coronavirus, in suspension or otherwise. We thus arrive at our understanding of pleomorphism through the colored lenses of electron microscopy, be it cryogenic fractography¹ or particle staining (Fig. 3. of Ref. 2). This is true whether the coronavirus capsid is axisymmetric or not. In cross section, as in microscopic imagery of microtomed coronavirus-infected tissue, a suspension of spherical capsids presents as circles, just circles. Further, when axisymmetric ellipsoidal coronavirus is sectioned, normal to its major axis (prolate), or to its minor axis (oblate), these cuts are also circular. Hence, in cross

section, a suspension of aspherical capsids presents as both circular and acircular loops. More specifically, a suspension of ellipsoidal capsids presents as both circles and ellipses. There is thus still much to be learned experimentally about the shape of the coronavirus. This paper is devoted to how its capsid shapes affect its transport properties.

General rigid bead-rod theory relies exclusively on macromolecular orientation to explain the rheological properties.³⁻⁷ This distinguishes general rigid bead-rod theory from its competing approaches, which include reptation or disentanglement. We refer the reader to Ref. 8 for the detailed derivation of the general rigid bead-rod theory, and specifically, to Sec. III of Ref. 8. We define the characteristic length, L , of our coronavirus bead-rod models as the separation of nearest bead centers. Our general rigid bead-rod theory symbols, dimensional and non-dimensional respectively, are listed in Tables I and II, which follow those of the corresponding textbook treatments (EXAMPLE 16.7-1 of Ref. 9 or EXAMPLE 13.6-1 of Ref. 10). We are attracted to general rigid bead-rod theory first, for its flexibility. We are attracted to general rigid bead-rod theory second, for the accuracy

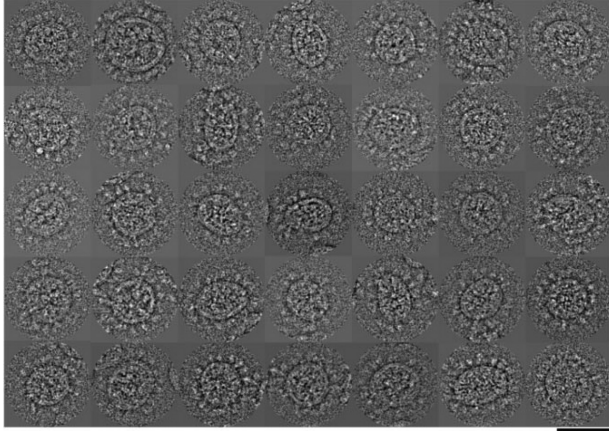


FIG. 1. Cryo-electron micrographs of pleomorphic SARS-CoV virions (Fig 2 of Ref. 1) Reproduced with permission from Neuman *et al.*, *J. Virol.* **80**, 7918 (2006).

of its simplest special case, the rigid dumbbell, for which many rheological material functions are properly predicted [see romanettes (i)–(xvi) of Sec. I of Ref. 11].

Recently, we calculated the rotational diffusivity of the spherical coronavirus in suspension, from first principles, using general rigid bead-rod theory.^{12–14} We did so by beading the spherical capsid and then also by replacing each of its bulbous spikes with a single bead

TABLE I. Dimensional variables. Legend: M —mass, L —length, and t —time.

Name	Unit	Symbol
Angular frequency	t^{-1}	ω
Augmented energy functional	ML^2/t^2	\widehat{E}
Bead friction coefficient	M/t	ζ
Capsid radius	L	r_c
Complex viscosity	M/Lt	η^*
Dielectric permittivity	$T^4 I^2 / ML^3$	ϵ
Kinetic molecular energy per molecule	ML^2/t^2	kT
Length of the spike of each peplomer	L	ℓ
Minus the imaginary part of the complex viscosity	M/Lt	η''
Number of dumbbells per unit volume	$1/L^3$	n
Point charge	$A s$	Q
Real part of the complex viscosity	M/Lt	η'
Relaxation time of rigid dumbbell	t	λ_0
Relaxation time of solution	t	λ
Rotational diffusivity	t^{-1}	D_r
Rotatory diffusivity	L^2/t	D_{rot}
Shear rate amplitude	t^{-1}	$\dot{\gamma}^0$
Solvent viscosity	M/Lt	η_s
Total electrostatic energy	ML^2/t^2	E
Translational diffusivity	L^2/t	D_{tr}
Virus radius	L	r_v
Viscosity, zero-shear	M/Lt	η_0
Zero-shear first normal stress difference	M/L	$\Psi_{1,0}$

TABLE II. Dimensionless variables and groups.

Name	Symbol
Aspect ratio	$\epsilon \equiv \frac{c}{a} - 1$
Capsid sphere	\mathcal{C}
Coefficient in Eqs. (9) and (10)	a
Coefficient in Eqs. (9) and (10)(9)	b
Coefficient in Eqs. (9) and (10)	ν
Deborah number, oscillatory shear	$De \equiv \lambda\omega$
Sphere	\mathcal{S}
Total number of beads	N
Total number of capsid beads	N_c
Total number of peplomers	N_p
Volume fraction	Φ
Weissenberg number	$Wi \equiv \lambda\dot{\gamma}^0$

(see Fig. 5 of Ref. 12). In this paper, we use energy minimization for the spreading of the spikes, charged identically, over the oblate or prolate capsids (Sec. IV). We use general rigid bead-rod theory to explore the role of such coronavirus cross-sectional ellipticity on its rotational diffusivity, the transport property around which its cell attachment revolves. We learn that coronavirus ellipticity decreases its rotational diffusivity for both oblate and prolate capsids.

In the tradition of the transport sciences, we define the rotatory diffusivity as (see Footnote 2 of p. 62 of Ref. 9)

$$D_{rot} \equiv \frac{2kT}{\zeta}, \tag{1}$$

which, for any axisymmetric macromolecule, from general rigid bead-rod theory, gives

$$D_{rot} \equiv \frac{12L^2}{\nu} D_r, \tag{2}$$

which has the dimensions of diffusivity and which is four times the translational diffusivity

$$D_{rot} \equiv 4D_{tr} \tag{3}$$

or

$$D_r \equiv \frac{\nu}{3L^2} D_{tr}. \tag{4}$$

In this paper, we depart from said transport tradition of using the rotatory diffusivity, D_{rot} , and frame our results in terms of the rotational diffusivities, D_r , of pleomorphic coronavirus particles.

II. METHOD

In general rigid bead-rod theory, we construct macromolecules from sets of beads whose positions, relative to one another, are fixed. Our macromolecular bead-rod models of our pleomorphic coronavirus particles are suspended in a Newtonian solvent. In this work, we neglect interactions of the solvent velocity fields, be they between nearest beads,^{15,16} or nearest macromolecules. With general rigid bead-rod theory, we thus locate beads to sculpt an approximation of the pleomorphic coronavirus particle shapes. In this way, using general rigid

bead-rod theory, we can model any virus macromolecular architecture (see Fig. 9 of Ref. 11).

We use Eqs. (3)–(13) in Ref. 12 for the method of computing the rotational diffusivity (see Footnote 2 of p. 62 of Ref. 9)

$$D_r \equiv \frac{1}{6\lambda} \tag{5}$$

or [Eq. (23) of Ref. 12]

$$\lambda_0 D_r = \frac{\nu}{72}, \tag{6}$$

which we will use for our results below.

III. OSCILLATORY SHEAR FLOW

In this paper, we focus on small-amplitude oscillatory shear flow (SAOS). For this flow field, for the molecular definition of small amplitude, general rigid bead-rod theory yields [Eq. (32) of Ref. 12]

$$\lambda \dot{\gamma}^0 \ll \frac{1}{\nu\sqrt{2}}, \tag{7}$$

whose left side is the macromolecular Weissenberg number.

The polymer contributions to the complex viscosity^{17,18}

$$\eta^* \equiv \eta' - i\eta'' \tag{8}$$

are [Eqs. (40) and (41) of Ref. 11]

$$\frac{\eta' - \eta_s}{\eta_0 - \eta_s} = \left(\frac{1}{2b/av} + 1 \right)^{-1} \left(\frac{1}{2b/av} + \frac{1}{1 + (\lambda\omega)^2} \right) \tag{9}$$

and

$$\frac{\eta''}{\eta_0 - \eta_s} = \left(\frac{1}{2b/av} + 1 \right)^{-1} \frac{\lambda\omega}{1 + (\lambda\omega)^2}, \tag{10}$$

where $\lambda\omega$ is the Deborah number. Equations (9) and (10) each capture non-Newtonian behavior: (i) Eq. (9) captures the descent of $\eta'(\omega)$ and (ii) Eq. (10) captures the ascent of $\eta''(\omega)$ from the origin. In this paper, we plot the real and *minus* the imaginary parts of the shear stress responses to small-amplitude oscillatory shear flow as functions of frequency, following Ferry (Secs. 2.A.4–2.A.6 of Ref. 19) or Bird *et al.* (Sec. 4.4 of Ref. 20):

As $\omega \rightarrow 0$, for the polymer contribution to the zero-shear viscosity, we get

$$\frac{\eta_0 - \eta_s}{nkT\lambda} = \frac{av}{2} + b = b \left[1 + \frac{2b}{av} \right] \left(\frac{2b}{av} \right)^{-1} \tag{11}$$

and for the zero-shear first normal stress difference coefficient

$$\frac{\Psi_{1,0}}{\lambda(\eta_0 - \eta_s)} = 2 \left(\frac{1}{2b/av} + 1 \right)^{-1}, \tag{12}$$

which we use in the table of Sec. V. below.

IV. MODELING OF ELLIPSOIDAL CORONAVIRUS

Coronavirus peplomers are charged identically and anchored into a lipid bilayer, and are thus displaced by the repulsions of their nearest neighbors. In this paper, we represent peplomers with single beads. We then locate them by applying the energy minimization

scheme of Sec. IV. of Ref. 13 to singly beaded peplomers repelling one another over ellipsoidal surfaces of the pleomorphic virus.

From the literature, we learn that if oblate, the coronavirus shape range is [Figs. 1(a) and 2 of Ref. 1]

$$\frac{2}{3} \leq \frac{c}{a} \leq \frac{4}{5}, \tag{13}$$

and if prolate [Figs. 1(a) and 2 of Ref. 1]

$$\frac{5}{4} \leq \frac{c}{a} \leq \frac{3}{2}. \tag{14}$$

For this work, we therefore cover [Eqs. (13) *plus* (14)]

$$\frac{5}{4} \leq \frac{c}{a} \leq \frac{4}{5}, \tag{15}$$

where, c is the ellipsoidal whole-particle length along the δ_3 molecular axis, and a along the δ_1 . By *whole-particle*, we mean capsid *plus* peplomer. Specifically, for this paper, we straddle both ranges Eqs. (13) and (14) with the following set of pleomorphic coronavirus aspect ratios

$$\frac{c}{a} = \left[\frac{2}{3}, \frac{4}{5}, 1, \frac{5}{4}, \frac{3}{2} \right] \tag{16}$$

for which, after energy minimization, we construct the bead-rod models of Figures 2–6 (Multimedia views) for $N_c = 256$ and $N_p = 74$. For the $N_c = 256$, we rely on the capsid beading study (see subsection VII A of Ref. 12). For the average number of peplomers, $N_p = 74$, we rely on our previous literature review (see Table X of Ref. 12).

We next employ the framework developed by Chaurasia *et al.*²¹ (see also Chaurasia²²) to find equilibrium solutions of a system consisting of flexible structures, specifically charged elastic loops constrained to a sphere. We do so for identical point charges spreading over the surfaces of oblate and prolate ellipsoids.

A. Kinematics

Let \mathcal{C} be the ellipsoidal capsid with axes lengths a , b , and c . Let o be the origin of a Cartesian coordinate system with an orthonormal

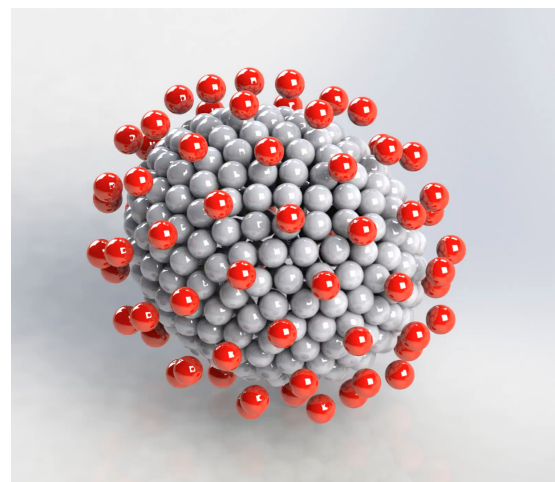


FIG. 2. General rigid bead-rod model of prolate coronavirus, $N_c = 256$, $N_p = 74$, and $c/a = 5/4$. Multimedia view: <https://doi.org/10.1063/5.0094771.1>

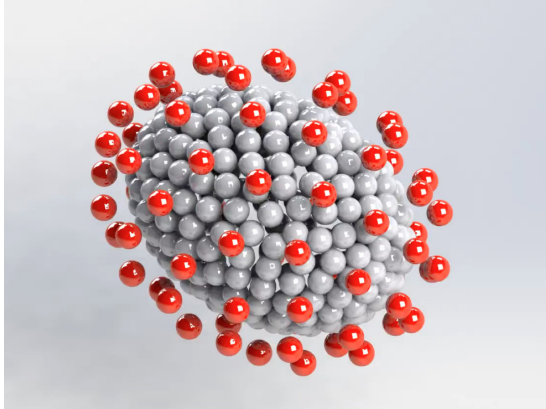


FIG. 3. General rigid bead-rod model of prolate coronavirus, $N_c = 256$, $N_p = 74$, and $c/a = 3/2$. Multimedia view: <https://doi.org/10.1063/5.0094771.2>

basis $\{i, j, k\}$, such that the center of \mathcal{C} coincides with the origin o and the axes of \mathcal{C} are along the vectors i, j , and k , respectively. Let N_p be the number of single bead peplomers of identical spike length ℓ attached along the normal to the ellipsoid \mathcal{C} at the point of contact. The point of contact of the i th bead to \mathcal{C} is defined by

$$x_i \mathbf{i} + y_j \mathbf{j} + z_i \mathbf{k}, \tag{17}$$

where $i = 1, 2, \dots, N$. Then, the quantities x_i, y_i , and z_i must satisfy

$$\frac{x_i^2}{a^2} + \frac{y_i^2}{b^2} + \frac{z_i^2}{c^2} = 1. \tag{18}$$

We assume that each peplomer spike is attached to the ellipsoidal capsid \mathcal{C} along the normal to \mathcal{C} . The normal vector at the point of contact $x_i \mathbf{i} + y_j \mathbf{j} + z_i \mathbf{k}$ of the spike of the i th peplomer to \mathcal{C} is given by

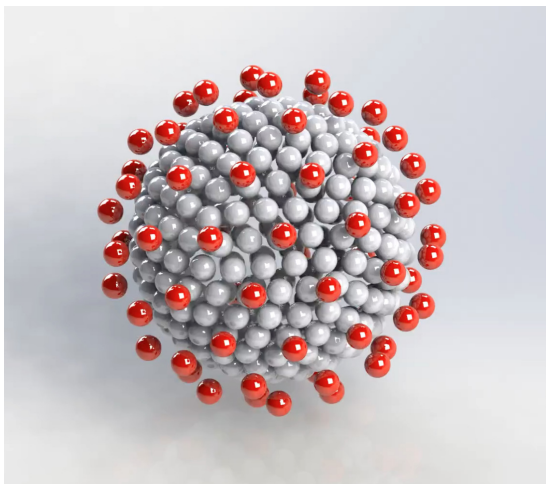


FIG. 4. General rigid bead-rod model of spherical coronavirus, $N_c = 256$, $N_p = 74$, and $c/a = 1$. Multimedia view: <https://doi.org/10.1063/5.0094771.3>

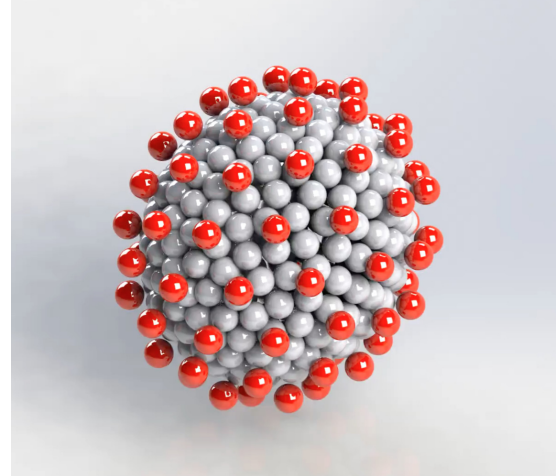


FIG. 5. General rigid bead-rod model of oblate coronavirus, $N_c = 256$, $N_p = 74$, and $c/a = 4/5$. Multimedia view: <https://doi.org/10.1063/5.0094771.4>

$$n_i \equiv \frac{x_i}{a^2} \mathbf{i} + \frac{y_i}{b^2} \mathbf{j} + \frac{z_i}{c^2} \mathbf{k} = 1. \tag{19}$$

Thus, introducing a scalar quantity $t_i, i = 1, 2, \dots, N$, the position vector r_i of the i th bead is given by

$$r_i \equiv x_i \mathbf{i} + y_j \mathbf{j} + z_i \mathbf{k} + t_i n_i, \tag{20}$$

where, by using Eq. (19), Eq. (20) simplifies to

$$r_i \equiv x_i \left(1 + \frac{t_i}{a^2}\right) \mathbf{i} + y_i \left(1 + \frac{t_i}{b^2}\right) \mathbf{j} + z_i \left(1 + \frac{t_i}{c^2}\right) \mathbf{k}, \tag{21}$$

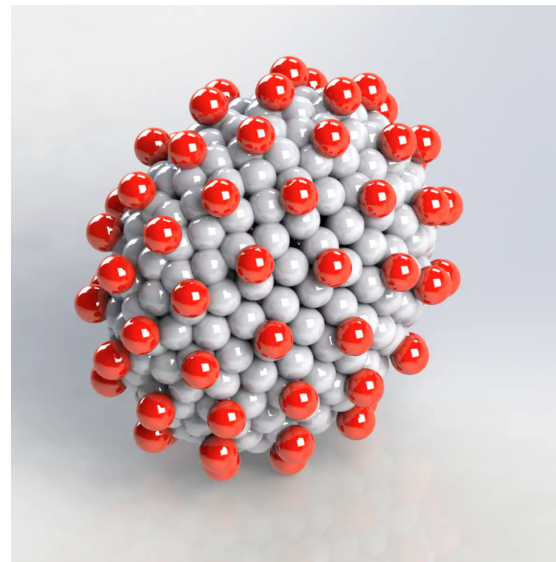


FIG. 6. General rigid bead-rod model of oblate coronavirus, $N_c = 256$, $N_p = 74$, and $c/a = 2/3$. Multimedia view: <https://doi.org/10.1063/5.0094771.5>

where $i = 1, 2, \dots, N$. We note from Eq. (21) that the length of the spike of the i th peplomer is given by $|r_i - (x_i \mathbf{i} + y_i \mathbf{j} + z_i \mathbf{k})| = |t_i n_i|$, $i = 1, 2, \dots, N$. For simplification, we assume that the length of the spike of each peplomer is equal to ℓ ; thus, the quantities x_i, y_i, z_i , and t_i and Eq. (19) of n_i in $|t_i n_i|^2 = \ell^2$ must satisfy

$$t_i^2 \left(\frac{x_i^2}{a^4} + \frac{y_i^2}{b^4} + \frac{z_i^2}{c^4} \right) = \ell^2, \tag{22}$$

where $i = 1, 2, \dots, N$. Thus, the position vector r_i , defined by Eq. (21), of the i th peplomer bead of a given spike length ℓ is entirely determined in terms of four scalar quantities x_i, y_i, z_i , and t_i satisfying Eqs. (18) and (22). For an axisymmetric capsid, $a = b$.

B. Energetics

Let each single bead peplomer be endowed with a point charge Q . The total electrostatic energy of N_p peplomers, constrained to the ellipsoidal capsid \mathcal{C} , is given by

$$E = \frac{Q}{4\pi\epsilon} \sum_{i=1}^N \sum_{j=1}^N \frac{1}{|r_i - r_j|}, \tag{23}$$

where ϵ is dielectric permittivity and r_i , defined in Eq. (21), is the position vector of the i th peplomer.²³

We have assumed that each bead is endowed with an identical point charge Q for simplification. Therefore, the beads repel each other and would prefer to distribute themselves as far as possible from each other to minimize the electrostatic energy E , defined in Eq. (23). Using a constrained minimization approach, we find an equilibrium distribution of the beads, defined in Eq. (20), that locally minimizes the energy in Eq. (23) while satisfying the kinematic constraints in Eqs. (18) and (22), for given values of N_p . Since the charge Q appears only as a prefactor in Eq. (23), its value plays no role in determining equilibrium solutions. Dropping that prefactor, we define the augmented energy functional

$$\begin{aligned} \hat{E}|r_i, \Lambda_i, \lambda_i|_{i=1, \dots, N_p} &= \sum_{i=1}^{N_p} \sum_{j=1}^{N_p} \frac{1}{|r_i - r_j|} + \frac{1}{2} \sum_{i=1}^{N_p} \Lambda_i \left(\frac{x_i^2}{a^2} + \frac{y_i^2}{b^2} + \frac{z_i^2}{c^2} - 1 \right) \\ &+ \frac{1}{2} \sum_{i=1}^{N_p} \lambda_i \left(t_i^2 \left(\frac{x_i^2}{a^4} + \frac{y_i^2}{b^4} + \frac{z_i^2}{c^4} \right) - \ell^2 \right), \end{aligned} \tag{24}$$

where using Eq. (21)

$$|r_i - r_j| = \sqrt{\begin{aligned} &\left[x_i \left(1 + \frac{t_i}{a^2} \right) - x_j \left(1 + \frac{t_j}{a^2} \right) \right]^2 \\ &+ \left[y_i \left(1 + \frac{t_i}{b^2} \right) - y_j \left(1 + \frac{t_j}{b^2} \right) \right]^2 \\ &+ \left[z_i \left(1 + \frac{t_i}{c^2} \right) - z_j \left(1 + \frac{t_j}{c^2} \right) \right]^2 \end{aligned}}, \tag{25}$$

where Λ_i and λ_i are the Lagrange multipliers introduced to satisfy the kinematic constraints in Eqs. (18) and (22). For finding the distribution of the beads locally minimizing the electrostatic energy E , defined

in Eq. (23), we differentiate the augmented energy functional, \hat{E} , with scalar quantities x_i, y_i, z_i , and t_i , where $i = 1, \dots, N_p$, resulting in $4N_p$ equilibrium equations

$$\sum_{\substack{j=1 \\ j \neq i}}^{N_p} \frac{(r_i - r_j) i \left(1 + \frac{t_i}{a^2} \right)}{|r_i - r_j|^{3/2}} - \frac{\Lambda_i x_i}{a^2} - \frac{\lambda_i t_i^2 x_i}{a^4} = 0, \tag{26}$$

$$\sum_{\substack{j=1 \\ j \neq i}}^{N_p} \frac{(r_i - r_j) j \left(1 + \frac{t_i}{b^2} \right)}{|r_i - r_j|^{3/2}} - \frac{\Lambda_i y_i}{b^2} - \frac{\lambda_i t_i^2 y_i}{b^4} = 0, \tag{27}$$

$$\sum_{\substack{j=1 \\ j \neq i}}^{N_p} \frac{(r_i - r_j) k \left(1 + \frac{t_i}{c^2} \right)}{|r_i - r_j|^{3/2}} - \frac{\Lambda_i z_i}{c^2} - \frac{\lambda_i t_i^2 z_i}{c^4} = 0, \tag{28}$$

and

$$\sum_{\substack{j=1 \\ j \neq i}}^{N_p} \frac{(r_i - r_j) n_i}{|r_i - r_j|^{3/2}} - \lambda_i t_i \left(\frac{x_i^2}{a^4} + \frac{y_i^2}{b^4} + \frac{z_i^2}{c^4} \right) = 0, \tag{29}$$

respectively, where n_i and r_i are defined by Eqs. (19) and (20). In total, we solve $6N_p$ equations, $4N_p$ equilibrium equations in Eqs. (26)–(29), and $2N_p$ constraints in Eqs. (18) and (22), simultaneously to determine $6N_p$ unknowns in $x_i, y_i, z_i, t_i, \lambda_i$, and Λ_i , where $i = 1, \dots, N_p$. We use the Levenberg–Marquardt algorithm from the *fsolve* package of MATLAB to solve the system of equations with 10^{-16} error tolerance.

General rigid bead-rod theory can be used either structure-by-structure (see TABLES V–XIII of Ref. 11) or analytically (see TABLE XV of Ref. 11). For large values of N_p , such as $N_p = 74$, Eq. (23) is applied numerically. Thus, the bead positions \mathbf{R}_i , are not derived, but rather we arrive at their floating-point approximations. Our exploration of pleomorphism is thus structure-by-structure.

Our model, which has an ellipsoidal core, amounts to a modified version of the Thomson problem,²⁴ wherein one seeks to find a state that distributes N_p electrons over a unit sphere as evenly as possible, with minimum electrostatic energy. Wales *et al.*,^{25,26} solved this problem, providing solutions for a large set of values of N_p . Our energy minimization recovers accurately the results of Wales^{25,26} for the Thomson solution (energy minimization over a spherical surface), as it should (see Sec. VII. of Ref. 12). As far as we know, we are the first to perform such an energy minimization over the surface of an ellipsoid.

V. RESULTS

Table III summarizes our results for the characteristics of ellipsoidal coronavirus particles, be they oblate or prolate, arrived at from general rigid bead-rod theory for $N_c = 256$ and $N_p = 74$. Figure 7 maps columns 2 and 3 of Table III onto the $I_3 - I_1$ plane, showing the balance of moments of each pleomorphic coronavirus bead-rod model. The oblate ones lie above the diagonal, and the prolate, below. The spherically symmetric coronavirus lies on the diagonal, near the origin. Figure 8 shows that pleomorphism, be it oblate or prolate, causes the real part of the complex viscosity, $\eta'(\omega)$, to descend with frequency. This is not seen for the spherical capsid (black horizontal line). In other words, pleomorphism introduces non-Newtonian behavior.

TABLE III. Ellipsoidal coronavirus particle characteristics from general rigid bead-rod theory with $N_c = 256$ and $N_p = 74$.

Coronavirus ellipsoid, c/a	$\frac{I_1}{mL^2}$	$\frac{I_2}{mL^2}$	$\frac{I_3}{mL^2}$	a	b	ν	$\frac{2b}{a\nu}$	$\frac{\eta_0 - \eta_s}{nkT\lambda}$	$\frac{\lambda}{\lambda_0}$	$\lambda_0 D_r$	$\frac{\Psi_{1,0}}{\lambda(\eta_0 - \eta_s)}$
1	1.06×10^6	1.06×10^6	1.46×10^6	5.66×10^5	8.70×10^{-2}	5.66×10^{-6}	5.43×10^{-2}	1.69	2.12×10^6	7.86×10^{-8}	2.10×10^{-1}
2	0.86×10^6	0.86×10^6	1.03×10^6	4.45×10^5	2.79×10^{-2}	7.10×10^{-6}	1.77×10^{-2}	1.61	1.69×10^6	9.86×10^{-8}	6.94×10^{-2}
3	4.98×10^5	4.98×10^5	3.15×10^5	2.05×10^5	8.11×10^{-2}	1.20×10^{-5}	6.56×10^{-2}	1.32	9.97×10^5	1.67×10^{-7}	2.46×10^{-1}
4	5.58×10^5	5.58×10^5	4.41×10^5	2.55×10^5	2.67×10^{-2}	1.07×10^{-5}	1.95×10^{-2}	1.39	1.12×10^6	1.49×10^{-7}	7.67×10^{-2}
5	2.48×10^2	2.48×10^2	2.48×10^2	1.24×10^2	1.19×10^{-8}	2.24×10^{-2}	7.96×10^{-9}	1.5	4.96×10^2	3.36×10^{-4}	1.60×10^{-8}

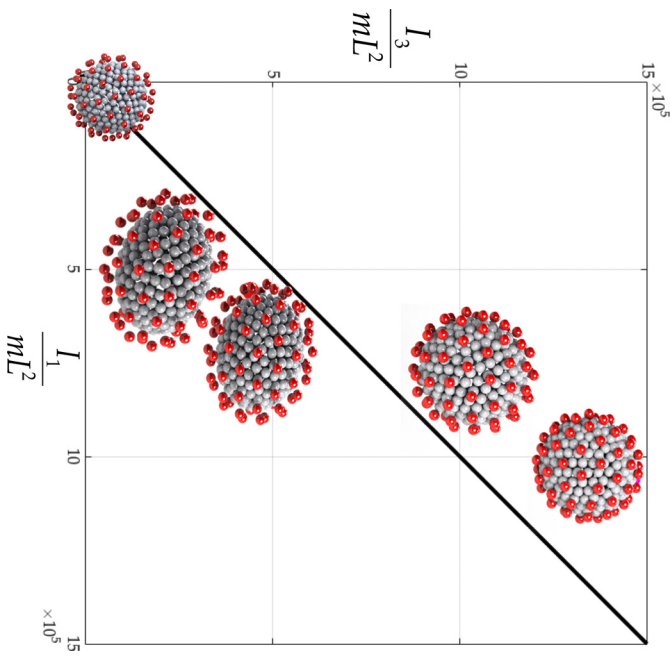


FIG. 7. $I_3 - I_1$ plane locating bead-rod models of pleomorphic coronavirus (from columns 2 and 3 of Table III), with the oblate ones lying above the diagonal ($I_3 > I_1$), the prolate, below ($I_3 < I_1$), and the spherical, near the origin ($I_3 = I_1$).

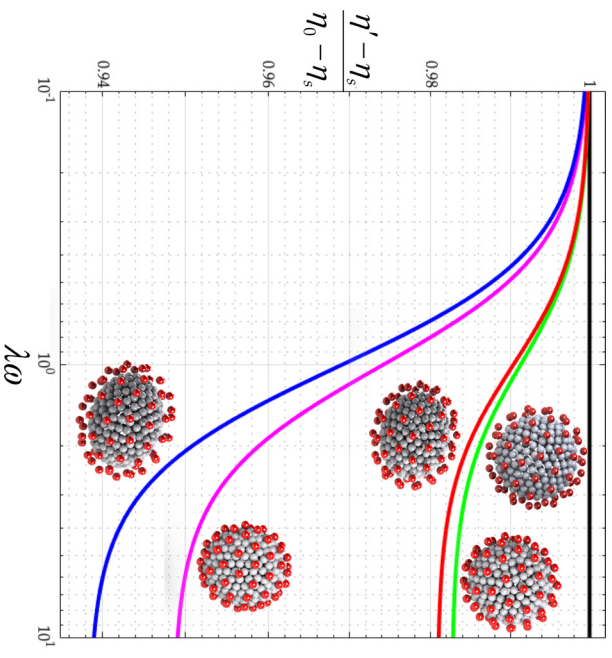


FIG. 8. Effect of ellipticity on the dimensionless real part of the complex viscosity, $\eta' - \eta_s/\eta_0 - \eta_s$, using Eq. (9), spherical $c/a = 1$ (black), prolate $c/a = 3/2$ (blue), prolate $c/a = 5/4$ (red), oblate $c/a = 2/3$ (magenta), and oblate $c/a = 4/5$ (green) ($N_c = 256$, $N_p = 74$, respectively, rows 1–4 of Table III).

Further, when compared with Fig. 10 of Ref. 12, Fig. 9 shows that pleomorphism, be it oblate or prolate, provokes an imaginary part to the complex viscosity, $\eta''(\omega)$. In other words, pleomorphism introduces elasticity to coronavirus suspensions. From Fig. 8, we also learn that when prolate coronavirus is compared to its oblate counterpart (where one ellipticity is the reciprocal of the other), the prolate decreases $\eta'(\omega)$ more than the oblate. Further, from Fig. 9, we learn that when prolate coronavirus is compared to its oblate counterpart (where one ellipticity is the reciprocal of the other), the oblate increases $\eta''(\omega)$ less than the prolate. Finally, Fig. 8 shows the order of descent for $\eta'(\omega)$ to be

$$\frac{c}{a} = \left[1, \frac{4}{5}, \frac{5}{4}, \frac{2}{3}, \frac{3}{2} \right], \tag{30}$$

and Fig. 9 shows the order of ascent for $\eta''(\omega)$ to be

$$\frac{c}{a} = \left[\frac{3}{2}, \frac{2}{3}, \frac{5}{4}, \frac{4}{5}, 1 \right], \tag{31}$$

which is the reverse of Eq. (30).

Figure 11 shows that pleomorphism, be it oblate or prolate, causes the dimensionless rotational diffusivity to decrease. Further, from Fig. 11 we learn that when prolate coronavirus is compared to its oblate counterpart (where one ellipticity is the reciprocal of the other), the oblate decreases the dimensionless rotational diffusivity more than the prolate. Figure 10 recalls the canonical dimensionless rotational diffusivity behavior of spherical coronavirus particles (Fig. 12 of Ref. 12 and Fig. 5 of Ref. 13). Comparing Fig. 10 to Fig. 11, we discover that with the reported pleomorphisms [Eq. (15)], $\lambda_0 D_r$ lands about 3 orders of magnitude below the canonical rotational diffusivity of spherical coronavirus. Finally, mindful of Fig. 11, Fig. 10 shows the order of descent for $\lambda_0 D_r$ to be

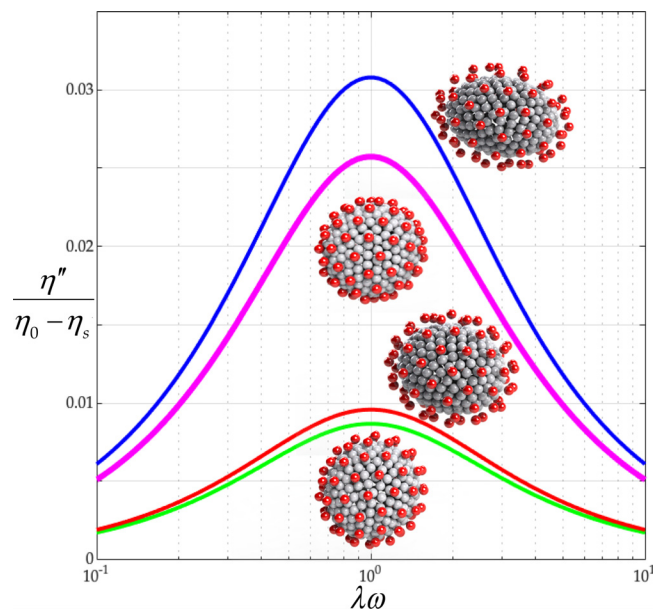


FIG. 9. Effect of ellipticity on the dimensionless minus the imaginary part of the complex viscosity, $\eta''/\eta_0 - \eta_s$, using Eq. (10), prolate $c/a = 3/2$ (blue), prolate $c/a = 5/4$ (red), oblate $c/a = 2/3$ (magenta), and oblate $c/a = 4/5$ (green) ($N_c = 256$, $N_p = 74$, respectively, rows 1–4 of Table III).

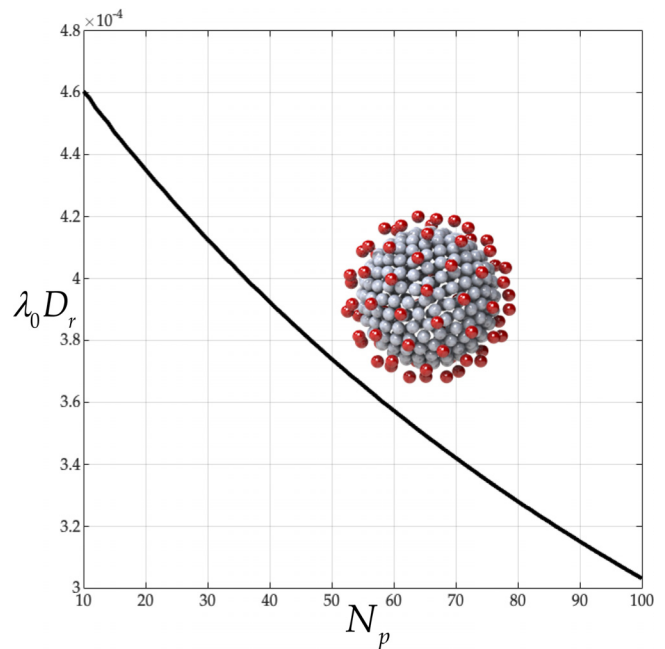


FIG. 10. Dimensionless rotational diffusivity $\lambda_0 D_r$, from Eq. (6) vs peplomer population N_p ($N_c = 256$). Spherical $c/a = 1$.

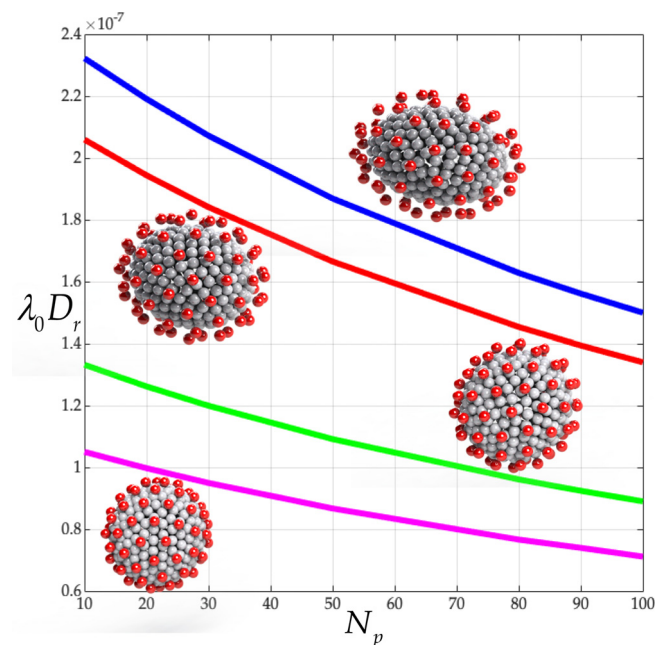


FIG. 11. Dimensionless rotational diffusivity $\lambda_0 D_r$, from Eq. (6) vs peplomer population N_p ($N_c = 256$). Prolate $c/a = 3/2$ (blue), prolate $c/a = 5/4$ (red), oblate $c/a = 2/3$ (magenta), and oblate $c/a = 4/5$ (green).

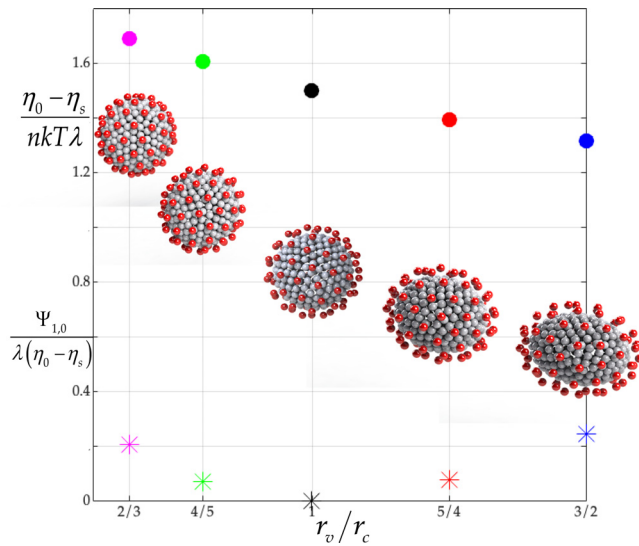


FIG. 12. Dimensionless zero-shear viscosity, η_0 , and zero-shear first normal stress difference coefficient, $\Psi_{1,0}$ from Eqs. (11) and (13), respectively, vs ellipticity. Spherical $c/a = 1$ (black), Prolate $c/a = 3/2$ (blue), prolate $c/a = 5/4$ (red), oblate $c/a = 2/3$ (magenta), and oblate $c/a = 4/5$ (green).

$$\frac{c}{a} = \left[1, \frac{3}{2}, \frac{5}{4}, \frac{4}{5}, \frac{2}{3} \right], \quad (32)$$

which differs from both Eqs. (30) and (31), and is not monotonic.

From column 8 of Table III and Fig. 12, we find that (i) oblate coronavirus pleomorphism increases the dimensionless zero-shear viscosity, η_0 , and (ii) prolate coronavirus pleomorphism decreases the dimensionless zero-shear viscosity. We also find, from column 11 of Table III and Fig. 12, that coronavirus pleomorphism, be it oblate or prolate, increases the zero-shear first normal stress coefficient, $\Psi_{1,0}$.

VI. CONCLUSION

Through the lens of general rigid bead-rod theory, we have explored the role coronavirus cross-sectional ellipticity on its rotational diffusivity, the transport property around which its cell attachment revolves. We find that coronavirus pleomorphism, be it oblate or prolate, injects into the complex viscosity (i) non-Newtonian behavior, and (ii) elasticity (Figs. 8 and 9, respectively). We also learn that when prolate coronavirus is compared to its oblate counterpart, (i) the prolate decreases $\eta'(\omega)$ more than the oblate, and (ii) the oblate increases $\eta''(\omega)$ less than the prolate. We find that (i) oblate coronavirus pleomorphism increases the dimensionless zero-shear viscosity, η_0 , and (ii) prolate coronavirus pleomorphism decreases the dimensionless zero-shear viscosity (column 8 of Table III). We also find that coronavirus pleomorphism, be it oblate or prolate, increases the zero-shear first normal stress coefficient, $\Psi_{1,0}$ (column 11 of Table III). We further find that rotational diffusivity decreases with coronavirus pleomorphism, be it oblate or prolate, and specifically that this descent is monotonic with the ratio of major to minor axis lengths, c/a (see Sec. IV A).

In this paper, we explored coronavirus pleomorphism using single beads to approximate the hydrodynamic resistance contributed by its spikes. However, from previous work, we know that the bulbous

triangular equidimensional shape of the coronavirus spikes reduces rotational diffusivity (see Figs. 2, 4, and 5 of Ref. 13). We leave the important combination of coronavirus pleomorphism with spike triangularity for another day.

Our previous work on the rotational diffusivity of coronavirus suspensions has excluded interferences of Stokes flow velocity fields between nearby spikes.^{12,13} We did so because no theory for incorporating hydrodynamic interactions in general rigid bead rod theory had been advanced. However, such a method for incorporating hydrodynamic interactions analytically has now been developed (Sec. III. of Ref. 27) and used (Sec. V. of Refs. 27 and 28). For the spherical capsid, this problem has also recently been attacked by means of molecular dynamics simulations.²⁹ We leave the exploration of how spike hydrodynamic interactions affect coronavirus rotational diffusivity for future work.

General rigid bead-rod theory can only be applied to suspensions for whom the suspended particle structure is known. Thus, general rigid bead-rod theory cannot be more accurate than our knowledge of this structure. Of coronaviruses, Bärkena *et al.* wisely observed: “As a result of their pleomorphic nature, our structural insight into the coronavirus is still rudimentary, and it is based mainly on 2D electron microscopy.” Table X of Ref. 12 summarizes what we know about the average values of the physical characteristics of coronavirus particles, and specifically, how we arrived at $N_p = 74$ to rely upon in this study. From this study, we can see that a distribution of particle ellipticities will result in a corresponding distribution of particle rotational diffusivities. The virus likelihood of attaching, we would expect, will be determined by this distribution. To handle such mixtures of different species, we can rewrite Eqs. (9) and (10) for a dispersed system (see problem14C.2 of Ref. 9, see also Sec. 26 of Ref. 30). We leave this for another day.

Though coronavirus pleomorphism is well-known, little is understood about its causes. Peplomer repulsions, for instance, might themselves deform the capsid. So might flow. Coronavirus pleomorphism may also reflect different asymmetrical arrangements of its capsid contents.³¹ Our work is silent on these important considerations.

Pleomorphism causes the peplomer spacing to differ over the oblate or prolate coronavirus surfaces. In as much as attachment requires the alignment of an adjacent peplomer pair with its nominally rectangular dimeric receptor, this pleomorphic peplomer spacing will complicate Eq. (2) of Ref. 12 for the attachment probability. In other words, the probability of finding a peplomer both (i) aligned with said receptor and (ii) matching the dimeric spacing of said receptor differs from place to place over the surface of a pleomorphic coronavirus.

The uninitiated may wonder why our bead-rod model employs an empty capsid. After all, the capsid contents are what causes disease. However, only the parts of the suspended particle resisted hydrodynamically by the surrounding Newtonian fluid can contribute to the resisted rotation and to the complex viscosity of the suspension. Thus, the rotational diffusivity of an empty capsid does not differ from a packed one. In general rigid bead-rod theory, only beads dragged through solvent can contribute to the rheology. Pieces of the macromolecule that are shielded from the surrounding solvent, such as capsid contents, are not to be counted in the general bead-rod model.

In this paper, we just considered axisymmetric pleomorphism, both oblate and prolate. We know of no characterization, microscopic or otherwise, detailed enough to distinguish oblate from prolate, or for that matter, asymmetric from axisymmetric. Moreover, we still know of no rheological characterization of the coronavirus suspension. We

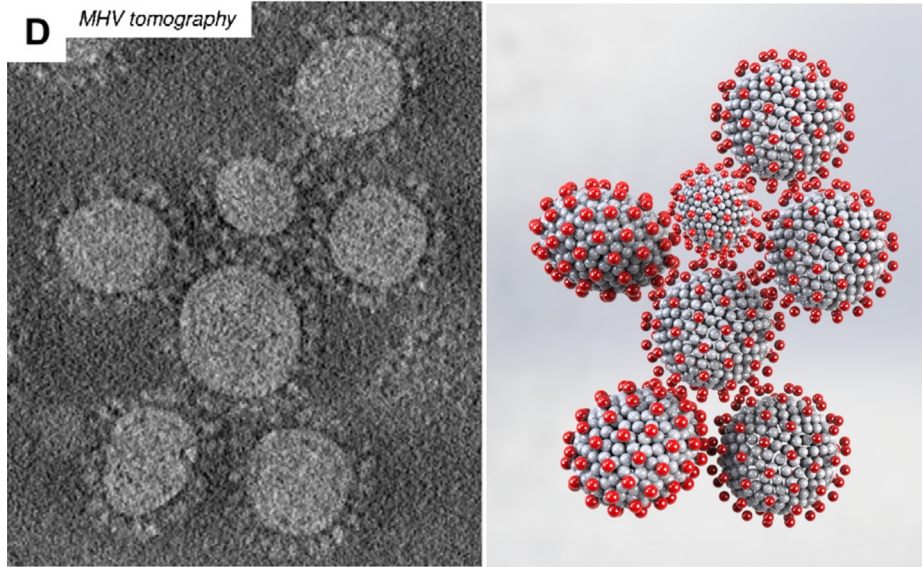


FIG. 13. Cryo-electron tomography of pleomorphic septocluster of interdigitated coronavirus (left) [Left panel of Fig. 1(d) of Ref. 35] vs our general rigid bead-rod pleomorphic model of same (right). Left panel reproduced with permission from B.W. Neuman, G. Kiss, G., A.H. Kunding, D. Bhella, M.F. Baksh, S. Connelly, B. Droese, J.P. Klaus, S. Makino, S.G. Sawicki, S.G. Siddell, "A structural analysis of M protein in coronavirus assembly and morphology," *J. Struct. Biol.* **174**(1), 11–22 (2011). Copyright 2011 Elsevier. Multimedia view: <https://doi.org/10.1063/5.0094771.6>

consider these experimental measurements to be crucial next steps for those equipped to handle live coronavirus.

Our general rigid bead-rod theory relies entirely on orientation to explain the polymer contribution to the viscosity and elasticity of polymeric liquids. Our theory is not to be confused with the competing theory, for suspensions of ellipsoids of revolution, which yields, for the real and *minus* the imaginary parts of the complex viscosity [after Eq. (11) of Ref. 34]

$$\frac{\eta' - \eta_s}{\eta_0 - \eta_s} = \frac{\frac{5}{2} + \frac{26}{147} \varepsilon^2 + \frac{3}{5} \frac{\varepsilon^2}{1 + \lambda^2 \omega^2}}{\frac{5}{2} + \frac{571}{735} \varepsilon^2}, \quad (33)$$

$$\frac{\eta''}{\eta_0 - \eta_s} = \frac{\frac{3}{5} \frac{\varepsilon^2 \lambda \omega}{1 + \lambda^2 \omega^2}}{\frac{5}{2} + \frac{571}{735} \varepsilon^2}, \quad (34)$$

where

$$\eta_0 - \eta_s = \eta_s \Phi \left[\frac{5}{2} + \frac{571}{735} \varepsilon^2 \right], \quad (35)$$

and where

$$\varepsilon \equiv \frac{c}{a} - 1, \quad (36)$$

where c/a is the capsid aspect ratio. Equations (33)–(36) are thus for suspensions of otherwise featureless ellipsoids (spikeless), be they prolate or oblate, arrived at elegantly through the competing ellipsoid suspension orientation theory. Unlike general rigid bead-rod theory, however, ellipsoid suspension orientation is silent on the relation between λ and the shapes and sizes of the suspended objects.

We have restricted this work to small-amplitude, namely, where Eq. (7) obtains. For large-amplitude oscillatory shear flow, where Eq. (7) does not obtain, we bridge to the corotational Jeffreys fluid,

following the method of Sec. X of Ref. 11. We leave this intriguing problem to future work.

Whereas much prior work on fluid physics related to the virus has attacked transmission,^{32,33} this paper focuses on the *ab initio* calculation of coronavirus transport properties. Specifically, we have determined the rotational diffusivity, the property governing the particle alignment for cell attachment (see Sec. I of Ref. 12). Although our work is mainly curiosity driven, it may deepen our understanding of drug, vaccine, and cellular infection mechanisms.

One might prefer to add other comparisons with experiment, and specifically with relevant complex viscosity vs coronavirus observations. However, we know of no experimental measurements on coronavirus suspensions. In other words, to our knowledge, the transport properties explored in this paper have yet to be explored in the laboratory.

Under the microscope, we see agglomeration of coronavirus particles, mechanically interlocked by interdigitation of the bulbous spikes [see Fig. 1(d) of Ref. 35]. The charge repulsion of the interdigitating spikes will, of course, rearrange the spikes. By *rearrange*, we mean spreading near the interdigitation, and crowding elsewhere. Figure 13 (Multimedia view) shows our general rigid bead-rod model of an interdigitated cluster of coronaviruses. We leave the energy minimization for interdigitated clusters, and the calculation of the coronavirus cluster rotational diffusivity for another day.

ACKNOWLEDGMENTS

This research was undertaken, in part, thanks to support from the Canada Research Chairs program of the Government of Canada for the Natural Sciences and Engineering Research Council of Canada (NSERC) Tier 1 Canada Research Chair in Rheology. This research was also undertaken, in part, thanks to support from the Discovery Grant program of the Natural Sciences and Engineering Research Council of Canada (NSERC) (A. J. Giacomin), Vanier Canada Graduate Scholarship (M. A. Kanso), and the Mitacs

Research Training Award (A. J. Giacomin and M. A. Kanso). A. J. Giacomin is indebted to the Faculty of Applied Science and Engineering of Queen's University at Kingston for its support through a Research Initiation Grant (RIG). V. Chaurasia and E. Fried gratefully acknowledge support from the Okinawa Institute of Science and Technology Graduate University with subsidy funding from the Cabinet Office, Government of Japan.

AUTHOR DECLARATIONS

Conflict of Interest

The authors have no conflicts to disclose.

DATA AVAILABILITY

The data that support the findings of this study are available from the corresponding author upon reasonable request.

REFERENCES

- ¹B. W. Neuman, B. D. Adair, C. Yoshioka, J. D. Quispe, G. Orca, P. Kuhn, R. A. Milligan, M. Yeager, and M. J. Buchmeier, "Supramolecular architecture of severe acute respiratory syndrome coronavirus revealed by electron cryo-microscopy," *J. Virol.* **80**(16), 7918 (2006).
- ²N. Zhu, D. Zhang, W. Wang, X. Li, B. Yang, J. Song, X. Zhao, B. Huang, W. Shi, R. Lu, P. Niu, F. Zhan *et al.*, "A novel coronavirus from patients with pneumonia in China, 2019," *N Engl. J. Med.* **382**(8), 727–733 (2020).
- ³M. A. Kanso, "Polymeric liquid behavior in oscillatory shear flow," M.S. thesis (Queen's University, Kingston, Canada, 2019).
- ⁴M. A. Kanso and A. J. Giacomin, "van Gorp-Palmen relations for long-chain branching from general rigid bead-rod theory," *Phys. Fluids* **32**(3), 033101 (2020); Erratum: In Eq. (44) " $I_3 > I_1$ " should be " $I_3 < I_1$." Editor's pick.
- ⁵M. A. Kanso, A. J. Giacomin, and C. Saengow, "Large-amplitude oscillatory shear flow loops for long-chain branching from general rigid bead-rod theory," *Phys. Fluids* **32**(5), 053102 (2020).
- ⁶M. A. Kanso, A. J. Giacomin, C. Saengow, and J. H. Piette, "Diblock copolymer architecture and complex viscosity," *Int. J. Mod. Phys. B* **34**, 2040110 (2020).
- ⁷D. Singhal, M. A. Kanso, S. J. Coombs, and A. J. Giacomin, "Complex viscosity of poly[n]catenanes and olympiades," *Phys. Fluids* **34**(3), 033112 (2022).
- ⁸O. Hassager, "Kinetic theory and rheology of bead-rod models for macromolecular solutions. II. Linear unsteady flow properties," *J. Chem. Phys.* **60**(10), 4001–4008 (1974); Erratum: in Eq. (2) of " $1/2$ " should be " $-1/2$ " and " \ll " should be " \gg ."
- ⁹R. B. Bird, C. F. Curtiss, R. C. Armstrong, and O. Hassager, *Dynamics of Polymeric Liquids* 2nd ed. (John Wiley & Sons, Inc., New York, 1987), Vol. 2; Errata: On p. 409 of the first printing, the $(n + m)!$ in the denominator should be $(n - m)!$; In Table 16.4–1, under L entry "length of rod" should be "bead center to center length of a rigid dumbbell"; In Fig. 14.1–2 caption, "Multibead rods of length L " should be "Multibead rods of length $L + d$."
- ¹⁰R. B. Bird, O. Hassager, R. C. Armstrong, and C. F. Curtiss, *Dynamics of Polymeric Liquids*, 1st ed. (John Wiley and Sons, Inc., New York, 1977), Vol. 2.
- ¹¹M. A. Kanso, A. J. Giacomin, C. Saengow, and J. H. Piette, "Macromolecular architecture and complex viscosity," *Phys. Fluids* **31**(8), 087107 (2019); Editor's pick. Errata: Ganged in Ref. 8 of Ref. 13.
- ¹²M. A. Kanso, J. H. Piette, J. A. Hanna, and A. J. Giacomin, "Coronavirus rotational diffusivity," *Phys. Fluids* **32**(11), 113101 (2020). Feature article. Cover article.
- ¹³M. A. Kanso, V. Chaurasia, E. Fried, and A. J. Giacomin, "Peplomer bulb shape and coronavirus rotational diffusivity," *Phys. Fluids* **33**(3), 033115 (2021).
- ¹⁴A. J. Giacomin and M. A. Kanso, "General rigid bead-rod macromolecular theory," in *Recent Advances in Rheology: Theory, Biorheology, Suspension and Interfacial Rheology*, edited by D. De Kee and A. Ramachandran (AIP Publishing, Melville, 2022), Chap. II, pp. 2–1–2–32.
- ¹⁵W. E. Stewart and J. P. Sørensen, "Hydrodynamic interaction effects in rigid dumbbell suspensions. II. Computations for steady shear flow," *Trans. Soc. Rheol.* **16**(1), 1–13 (1972).
- ¹⁶J. H. Piette, L. M. Jbara, C. Saengow, and A. J. Giacomin, "Exact coefficients for rigid dumbbell suspensions for steady shear flow material function expansions," *Phys. Fluids* **31**(2), 021212 (2019); Erratum: Above Eq. (83), "one other" should be "one other use."
- ¹⁷R. B. Bird and A. J. Giacomin, "Who conceived the complex viscosity?," *Rheol. Acta* **51**(6), 481–486 (2012).
- ¹⁸A. J. Giacomin and R. B. Bird, "Erratum: Official nomenclature of The Society of Rheology," *J. Rheol.* **55**(4), 921–923 (2011).
- ¹⁹J. D. Ferry, *Viscoelastic Properties of Polymers*, 3rd ed. (Wiley, New York, 1980).
- ²⁰R. B. Bird, R. C. Armstrong, and O. Hassager, *Dynamics of Polymeric Liquids*, 1st ed. (Wiley, New York, 1977), Vol. 1.
- ²¹V. Chaurasia, Y.-C. Chen, and E. Fried, "Interacting charged elastic loops on a sphere," *J. Mech. Phys. Solids* **134**, 103771 (2020).
- ²²V. Chaurasia, "Variational formulation of charged curves confined to a sphere," Ph.D. thesis (University of Houston, Houston, 2018).
- ²³J. Nocedal and M. L. Overton, "Projected Hessian updating algorithms for nonlinearly constrained optimization," *SIAM J. Numer. Anal.* **22**(5), 821–850 (1985).
- ²⁴J. Thomson, "XXIV. On the structure of the atom: An investigation of the stability and periods of oscillation of a number of corpuscles arranged at equal intervals around the circumference of a circle; with application of the results to the theory of atomic structure," *London, Edinburgh, Dublin Philos. Mag. J. Sci.* **7**(39), 237–265 (1904).
- ²⁵D. J. Wales and S. Ulker, "Structure and dynamics of spherical crystals characterized for the Thomson problem," *Phys. Rev. B* **74**(21), 212101 (2006).
- ²⁶D. J. Wales, H. McKay, and E. L. Altschuler, "Defect motifs for spherical topologies," *Phys. Rev. B* **79**(22), 224115 (2009).
- ²⁷M. C. Pak, K.-I. Kim, M. A. Kanso, and A. J. Giacomin, "General rigid bead-rod theory with hydrodynamic interaction for polymer viscoelasticity," *Phys. Fluids* **34**(2), 023106 (2022).
- ²⁸M. A. Kanso, M. C. Pak, K.-I. Kim, S. J. Coombs, and A. J. Giacomin, "Hydrodynamic interaction and complex viscosity of multi-bead rods," *Phys. Fluids* **34**(4), 043102 (2022). Editor's pick.
- ²⁹N. Moreno, D. Moreno-Chaparro, F. B. Usabiaga, and M. Ellero, "Hydrodynamics of spike proteins dictate a transport-affinity competition for SARS-CoV-2 and other enveloped viruses," bioRxiv (2022).
- ³⁰R. B. Bird, H. R. Warner, and D. C. Evans, "Kinetic theory and rheology of dumbbell suspensions with Brownian motion," *Fortschr. Hochpolym.-Forsch.* **8**, 1–90 (1971).
- ³¹P. J. de Pablo and I. A. T. Schaap, "Atomic force microscopy of viruses," in *Physical Virology*, edited by U. F. Greber (Springer, Cham, 2019) Chap. VIII, pp. 159–179.
- ³²T. Dbouk and D. Drikakis, "On coughing and airborne droplet transmission to humans," *Phys. Fluids* **32**(5), 053310 (2020).
- ³³H. Wang, Z. Li, X. Zhang, L. Zhu, Y. Liu, and S. Wang, "The motion of respiratory droplets produced by coughing," *Phys. Fluids* **32**(12), 125102 (2020).
- ³⁴L. G. Leal and E. J. Hinch, "The rheology of a suspension of nearly spherical particles subject to Brownian rotations," *J. Fluid Mech.* **55**(4), 745–765 (1972).
- ³⁵B. W. Neuman, G. Kiss, G., A. H. Kunding, D. Bhella, M. F. Baksh, S. Connelly, B. Droese, J. P. Klaus, S. Makino, S. G. Sawicki, and S. G. Siddell, "A structural analysis of M protein in coronavirus assembly and morphology," *J. Struct. Biol.* **174**(1), 11–22 (2011).